DOI: 10.61782/fa.2023.0603

forum acusticum 2023

INVESTIGATING THE EFFECT OF WOODWIND INSTRUMENT TONE HOLE SIZE USING PARTICLE IMAGE VELOCIMETRY

Titas Lasickas[1*] **Giuseppe Carlo Alp Caridi**[2] **Alfredo Soldati**[2,3] **Vasileios Chatziioannou**[1]

[1] Department of Music Acoustics, University of Music and Performing Arts Vienna, Austria
[2] Institute of Fluid Mechanics and Heat Transfer, Vienna University of Technology, Austria
[3] Polytechnic Department, University of Udine, Italy

ABSTRACT

An experimental study is conducted to analyse the influence of tone hole (TH) size on the pitch of woodwind instruments. Time-resolved Particle Image Velocimetry (PIV) is used to measure the velocity fluctuations and the natural frequencies of the resonator inside a simplified recorder. The sound is generated using a real mouthpiece, and the airflow has the same intraoral conditions as during human performance. PIV measurements are validated with pressure measurements obtained from pressure transducers. Four tone hole diameters are considered, ranging from 0.3 to 0.8 times the diameter of the bore. The results show local peaks of the velocity fluctuations in the proximity of the TH. At the open end of the instrument, the amplitude of the velocity fluctuations reduces with the size of the TH. Finally, a quadratic law between the first harmonic of the natural frequencies and the TH diameter was observed.

Keywords: *Woodwind instrument, Tone holes, PIV, Acoustic flow*

1. INTRODUCTION

Sound generation in flute-like instruments relies on the acoustic interaction of an oscillating air jet and the vibrations of an air column enclosed in the bore of the instrument. The oscillating jet can be considered as a localised amplifying element (source), driving the generation of standing waves in the air column (resonator) [1].

The geometry of the bore and the configuration of tone holes (THs), also known as finger holes, define the natural frequencies (resonant modes) in which the acoustic energy is accumulated. The lowest note a woodwind instrument can generate depends on the oscillating regime induced by the entire air column. Successively, higher notes are produced by opening holes one by one along the tube, beginning with the one farthest from the mouthpiece. This successive opening of holes shortens the effective length of the air column, which raises the frequencies of its modes [2]. Musicians can manipulate the pitch of the instrument by selectively opening and closing specific tone holes. [1] In addition, the effective length of the air

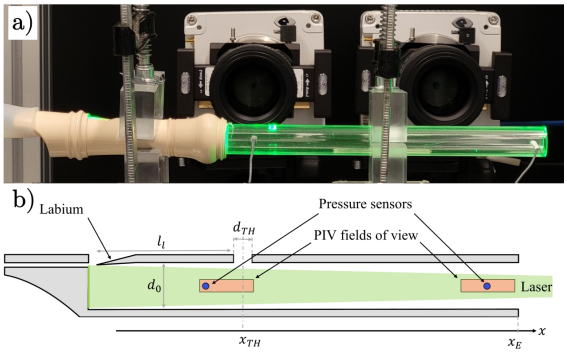

Figure 1: a) Picture of the experimental setup. b) Sketch of the recorder with the location of the pressure transducers (blue dots) and PIV field of view (red windows).

**Corresponding author*: *lasickas@mdw.ac.at.*

[1] Pitch modulation via embouchure modifications or overblowing is also common, but not considered in this work.

column (thus the pitch) is influenced by the location and geometry of the tone hole, as well as the bore geometry at that location [3,4]. Tone holes have varying diameters and depths that are usually determined by the thickness of the bore wall. Acoustic measurements in bores with a single tone hole have been used to characterise the effect of the TH using a physics-based model [5, 6]. Nevertheless, a complete analysis of the acoustic effects of the tone hole geometries is still missing.

The influence of THs is commonly studied by means of mathematical models. Specifically, the frequencies, magnitudes, and harmonicity can be retrieved by the input impedance or reflectance of the instrument using the transfer matrix method (TMM) [7, 8]. In the presence of tone holes, wave propagation can be resolved using modal decomposition [9, 10], finite difference methods (FDM) [3], and finite element methods (FEM) [11]. However, in the case of jet-driven musical instruments, it is difficult to predict the non-linear input of the acoustic source to solve the resonator response. The knowledge of fluid-acoustic interaction can overcome these limitations. To this end, experimental measurements, such as Particle Image Velocimetry (PIV), and numerical flow simulations, through Direct Numerical Simulations (DNS), within the instrument may improve the accuracy and reliability of the models used to simulate tone holes [1].

To date, there are few studies about the fluid-acoustic interaction. Most of these studies are focused on the location where the airflow instabilities take place (e.g., on the reed in a saxophone or on the labium in a recorder) exciting standing waves and producing sound waves [1, 12]. Even less material is found in the literature about the aeroacoustic effects of the TH geometry. Yokoyama et al. [13] have analysed the effect of the tone hole configuration on the standing waves by means of DNS and PIV measurements (non-time-resolved). Other authors have studied local effects, such as non-linear losses (e.g., boundary layer separation, vortex shedding and jet streaming), in the proximity of the TH [14–16]. The latter studies have employed PIV measurements in pipes connected to loudspeakers to simulate the behaviour of wind instruments. While this is a valuable approach, it lacks realistic excitation of the instrument, where the mean flow is present. Mean flow can affect the flow at the tone hole by generating vortices that vary in size over time and shed [17] as well as high amplitude pulsations in closed side branch systems, as observed in industrial applications [18]. To include these effects, the mean flow should be present during the experiments. In addition, to the authors' knowledge, the exact influence of the TH dimension on the airflow field is still missing.

The current investigation aims at characterising the effect of the TH size on the resonator response inside a simplified recorder. The sound is generated using a real mouthpiece, where the air flows with the same intraoral conditions as during human performance. Time-resolved PIV measurements at 15.5 kHz are used to detect and quantify the variation of the velocity fluctuations for four different TH diameters. The results provide the correlation between the fundamental frequencies and the size of the tone hole.

2. EXPERIMENTAL SETUP

2.1 Recorder geometry and flow

Experiments are conducted in the laboratories of the Institute of Fluid Mechanics and Heat Transfer at TU Wien and of the Department of Music Acoustics at the University of Music and Performing Arts Vienna. [2] The measurements are performed in a transparent tube mounted to a conventional recorder mouthpiece, as shown in Figure 1a. The inner diameter, $d_0 = 12$ mm, the length, $l = 19.9$ cm and the wall thickness, $h = 3$ mm, are chosen to be close to that of a commercial recorder, although the characteristic conical geometry has been simplified to a cylindrical one for practical reasons. The tone hole is located at a distance of $l_l = 11$ cm from the labium of the mouthpiece (see Fig. 1b). The experiments were performed with four different tone hole diameters in open and closed TH configurations. The tone hole sizes were $d_{\mathrm{TH}} = 4$ mm, 6 mm, 8 mm and 10 mm.

The airflow was generated by a compressor with a reservoir of 500 litres to ensure a constant flow rate during the measurements. The inlet pressure was set to 100 Pa to reproduce the intraoral pressure while playing a flute [19].

2.2 Measurement equipment and settings

In order to analyse the influence of the tone hole diameter, we measured the acoustic airflow velocity and pressure affected by the tone hole. The flow velocity was measured using a two-dimensional time-resolved PIV system, while the pressure was measured by means of pressure transducers. The location of the measurements are depicted in Fig. 1b. The first PIV window was placed around one of the expected acoustic velocity maxima, which is at the

[2] Data is available at https://iwk.mdw.ac.at/h2020-vrace/.

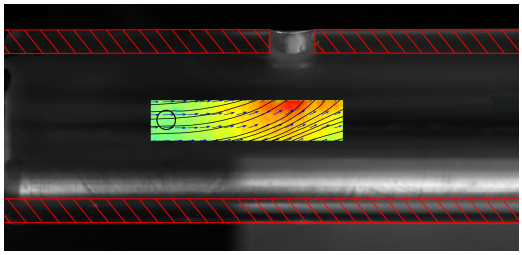

Figure 2: Field of view of the PIV measurements with respect to the bore size of the recorders. Red lines highlight the edges of the recorder and the circle represent the position of the microphone.

opening of the tone hole. In the reference system of the PIV measurements, the centre of the THs corresponds to $x_{\mathrm{TH}} = 11$ mm. The second window would be, ideally, extending outside the open end of the bore. However, to ensure homogeneous seeding concentration and to avoid the optical discontinuity of the outer edge, the second window was placed inside the recorder, close to its open end. The pressure transducers were placed within the PIV field of view for a better comparison. The need to remove and reallocate the tube in order to enlarge the tone hole for the next measurement set resulted in a slight displacement of the PIV windows. However, the PIV results for the different tone hole configurations are presented aligned with respect to the tone hole centre for a better comparison.

The PIV setup consists of a high-speed laser (527 nm, double cavity, 25 mJ per pulse, Litron LD60-532) and two high-speed cameras (Phantom VEO 340 L). The laser-sheet, of approximately 1 mm thickness, was arranged in order to enter the recorder from downstream to illuminate both fields of view at the same time without applying a width aperture. As a result, the light intensity was high enough to detect the 2 μm seeding tracers made with SAFEX fog fluid. Due to this light configuration, the laser-sheet was impinging perpendicularly on the inner surface of the mouthpiece's block (see Fig. 1b). Given the risk of burning the mouthpiece with a focused narrow sheet from a high-power laser, low-cost Aulos model 303A-E recorder mouthpieces were used.

The active area of the cameras' sensor was cropped to 900×200 pixels to obtain an acquisition frequency of 15500 Hz in order to fully resolve the acoustic fluctuations of the flow. The cameras were equipped with 100 mm focal length *Macro* objectives. At the set magnification of $M = 0.18$, the field of view (FOV) was 15.8×3.3 mm, which yielded a digital imaging resolution of 56.11 pixel/mm. It is worth mentioning that the optical distortion due to the pipe curvature is negligible thanks to the small height of the FOV with respect to the bore diameter and due to the FOV being centred with the instrument's axis, as can be seen from the scaled image of Fig. 2, where a sample of velocity contour with streamlines is over-imposed on the non-cropped image taken from the PIV camera.

The pressure measurements were carried out using Endevco 8507C-2 pressure transducers. These are provided already calibrated by the manufacturer. The advantage of this particular model relies on the accurate measurements even at high-pressure levels, which are typical in the interior of wind instruments. The transducers are placed flush with the inner wall of the tube, so that they do not significantly affect the flow. An amplifier (Endevco model 136) and a National Instrument IO board complete the pressure acquisition system. The acquisition of the pressure data was performed at 50 kHz for approximately one minute, within which the PIV images are acquired for a time duration of 1.3 seconds.

2.3 Data Processing

The flow velocity analysis was based on the inspection of 20,000 consecutive frames per TH configuration. The acquisition was performed using the software LaVision DaVis 10.2.1. Before computing velocity vectors, PIV images were pre-processed applying a sliding minimum subtraction (kernel: of 13 time-steps) and a spatial intensity normalisation with local average (computed over 50×50 pixels) to correct for light sheet non-uniformities and to reduce the background noise. The velocity fields are obtained using the software PaIRS-UniNa 0.1.2. A final interrogation window of 16×16 pixels was set to ensure the presence of 6 to 8 seeding particles. The universal outlier detection was also implemented with a kernel of 7×7 vectors, a minimum normalisation level set to 0.1 pixels, and a threshold value of 2 [20].

The root-mean-square (RMS) of the velocity is computed after subtracting the moving average with a kernel size of 50 frames, which corresponds to a high-pass filter with a cut-off frequency of 300 Hz. This procedure is performed in order to neglect low-frequency fluctuations which are not related to the pressure or acoustic fluctuations, as will be shown in Section 3.1.

3. RESULTS

This section shows the effects of the TH size on the flow velocity inside the simplified recorder. In particular, the results quantify the influence of the TH opening on the velocity fluctuations and on the power spectra computed from the PIV measurements.

3.1 Pulsating behaviour at the tone hole location

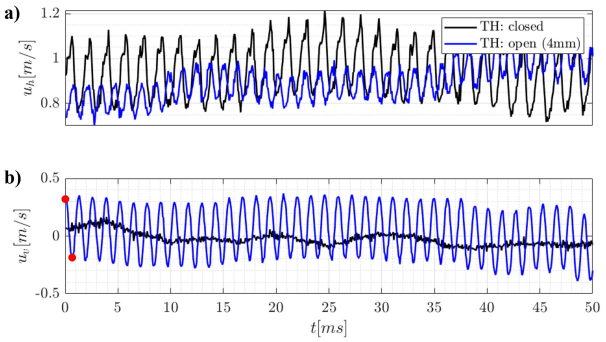

Figure 3: Horizontal (a) and vertical (b) component of the velocity for the closed and open tone hole (for the case of $d_{\mathrm{TH}} = 4$ mm). Red dots show the time instants used in Fig. 4.

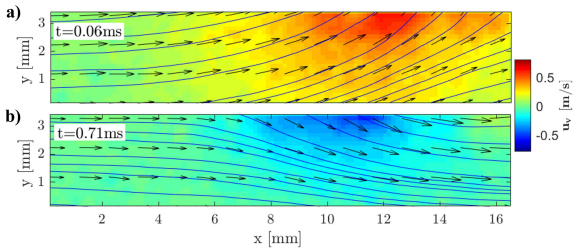

Figure 4: Contour of the vertical velocity U_v and streamlines at the maximum (a) and minimum (b) peak of the period for the case of $d_{\mathrm{TH}} = 4$ mm.

The flow velocity fluctuations measured at $x = x_{\mathrm{TH}}$ are presented in Fig. 3. For clarity, only a time interval of 50 ms of the velocity evolution is shown. As expected, for a closed tone hole, the fluctuations appear only in the horizontal component of the velocity. When the TH hole is open, an upward-downward velocity fluctuation appears at the location of the TH. As a consequence, a fluctuation of the vertical component of the velocity occurs while the amplitude of the horizontal component fluctuation diminishes.

The effect of the upward and downward pulsation is highlighted in Fig. 4. The streamlines computed at the maximum and minimum peak of the period (red dots in Fig. 3b) reveal an outflow and inflow from the tone hole during the pulsation driven by the jet streaming phenomenon, as documented in the literature [1, 16].

3.2 Velocity fluctuation

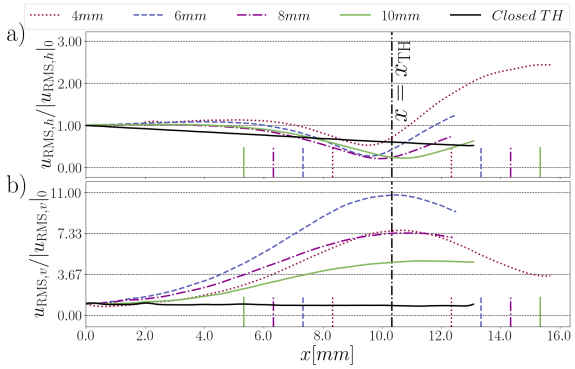

Figure 5: RMS of the velocity for the horizontal (a) and vertical (b) component computed at the location of the TH (FOV left in Fig. 1b). Values are normalised by the initial value $|u_{\mathrm{RMS}}|_0$. Vertical lines define the extension of the TH aperture.

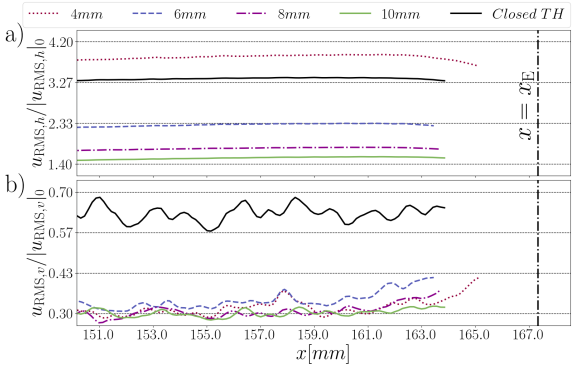

Figure 6: RMS of the velocity for the horizontal (a) and vertical (b) component near the open end (x_{E}) of the instrument (FOV right in Fig. 1b). Values are normalised by the initial value $|u_{\mathrm{RMS}}|_0$.

The effect of the jet streaming on the airflow fluctuations depends on the TH size. Figures 5 and 6 show the intensity of the velocity fluctuations in terms of root-mean-square for the left and right FOV in Fig. 1b. The

values of the RMS are computed and normalised by the initial value $|u_{\mathrm{RMS}}|_0$, which is measured at $x = 0$ mm. As a result, it is possible to compare the variation of the RMS along the axis with respect to the excitation magnitude for all TH configurations in both observation windows.

In the TH window (Fig. 5), a slight decrease in RMS is noted in the bore of the instrument for the closed TH case. In open TH configurations, the RMS reduces for the horizontal component and increases in the location of the TH, as mentioned in the previous paragraph. In addition, Fig. 5 shows that after the drop, $u_{\mathrm{RMS},h}/|u_{\mathrm{RMS},h}|_0$ increases, reaching higher values compared to the closed TH configuration, in particular for the smaller tone holes (i.e., $d_{\mathrm{TH}} = 4$ and 6 mm). This can be ascribed to local flow perturbations triggered by the tone hole, such as vortex shedding and oscillation of the recirculation region evolving downstream the TH, as documented in [15]. Unfortunately, the latter phenomena occur in the proximity of the TH edges which are outside the field of view of the present PIV measurements and additional measurements are needed for a complete discussion.

Near the outlet (Fig. 6), the value of the horizontal component of the RMS increases, as expected in an open acoustic pipe. In particular, for the closed TH $u_{\mathrm{RMS},h}/|u_{\mathrm{RMS},h}|_0$ has tripled. The aperture of the tone hole reduces the intensity of the horizontal velocity fluctuation at the edge of the bore. This is ascribed to the reduction of the pressure difference between the TH position ($x = 10.33$ cm) and the outlet ($x = 167.5$ mm) while the size of the TH increases.

Figure 7 shows the contours of the horizontal and vertical components of the RMS velocity for different tone hole diameters. The longitudinal coordinate is normalised by the diameters of the THs, effectively scaling the x-axis by the tone hole size, which allows a more direct comparison of the contours. The two-dimensional distributions of the RMS in Fig. 7 show regions of high intensity which extend from the TH. In the contour of the horizontal component, these regions diverge from the TH enveloping a low-intensity pseudo-conical region, while the intensity decreases going downwards (Fig. 7a). Instead, a spherical distribution, with the centre coinciding with that of the tone hole ($\chi/d_{\mathrm{TH}} = 0$), characterises the vertical component of the RMS (Fig. 7b).

3.3 Effect of the TH size on the frequency content

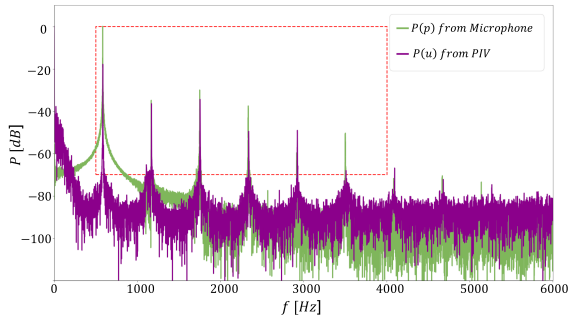

Figure 8: Comparison between the power spectrum in decibels computed from the PIV velocity, $P(u)$, and from pressure $P(p)$ for the closed tone hole. Red dashed widow represents the bounds of the ensuing plots in Fig. 9.

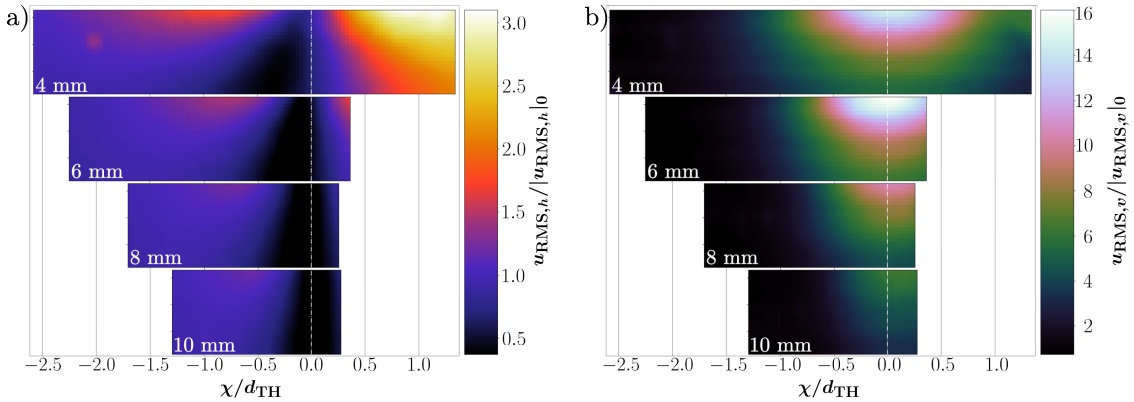

Figure 7: Contours of the horizontal (a) and vertical (b) component of root mean squared velocity for different apertures of the TH. For every case, the longitudinal coordinate χ is normalised by the diameters of the THs. The vertical dash-dotted line represents the centre of the tone hole. χ is the new longitudinal coordinate with the origin at the centre of the TH.

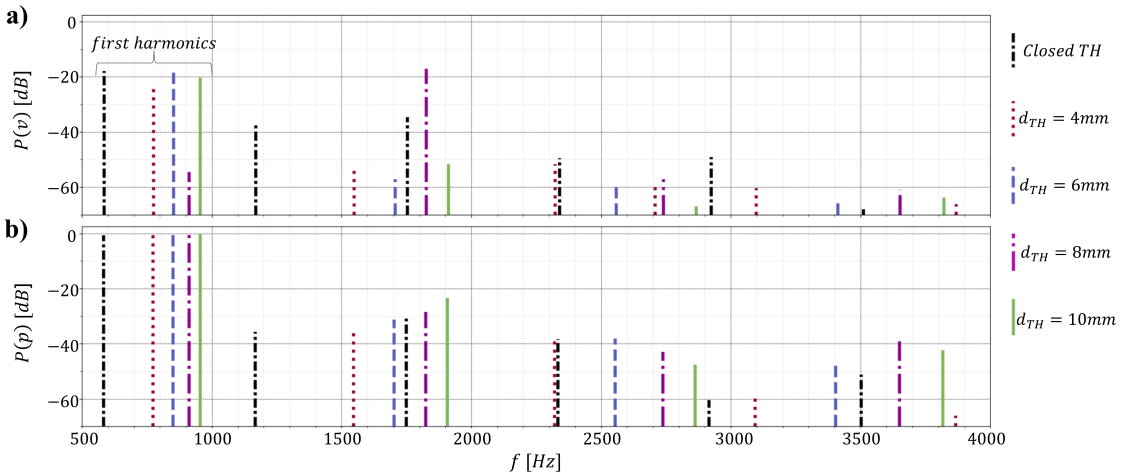

Figure 9: Power spectra peaks computed from the PIV velocity (a) and from the pressure measured by the microphone (b) for different TH configuration

The power spectra distributions obtained with the PIV measurements are in agreement with those captured by the pressure sensors. Fig. 8 compares the full power spectrum obtained from the two different measurements for the closed TH configuration. The spectra of the velocity are computed at the location of the first microphone for a more reliable comparison. It is shown that the main peaks almost overlap for the first six harmonics. The only discrepancy appears in the low frequency region ($f < 300$ Hz) where the PIV signal is not reliable due to the short acquisition time (1.3 seconds). For this reason, the comparison between all TH configurations considers only the dashed region depicted in Fig. 8 where the main peaks appear. In addition, the spectra obtained from the pressure do not show any dominant frequencies of interest in the region between 0 and 500 Hz in any of the TH configurations. It is worth mentioning that there is an additional peak at 2708 Hz in the horizontal air velocity magnitude spectrum in the case of the 4 mm open tone hole. This peak does not appear in the pressure measurement.

When the TH is closed, the first harmonic appears at 585 Hz, while opening the tone hole with a $d_{\mathrm{TH}} = 4$ mm the first harmonic reaches the value of 775 Hz. Increasing the section of the tone hole to d_{TH} = 6, 8, and 10 mm the fundamental frequency further increases to 853, 913, 956 Hz, respectively, as shown in Fig. 9. For completeness, the shift of the secondary harmonics that arise is also shown. The comparison of panel (a) and panel (b) of Fig. 9 confirms the agreement between the PIV measurements and the ones obtained with the pressure transducers also for the secondary harmonics.

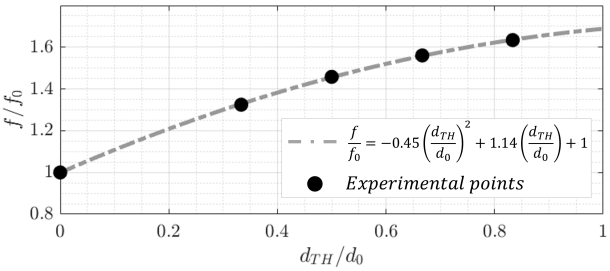

Figure 10: Scaling law of the first harmonic frequency in respect to the diameter of the TH, normalized by the diameter of the bore, d_0. The frequency is normalized by the value obtained with the closed TH configuration ($f_0 = 585$ Hz).

Configuration	f [Hz]	Note	Deviation [Cents]
Closed TH	585	$D5$	$+21$
$d_{\mathrm{TH}} = 4$ mm	775	$G5$	-36
$d_{\mathrm{TH}} = 6$ mm	853	$G\#5$	$+30$
$d_{\mathrm{TH}} = 8$ mm	913	$A5$	$+48$
$d_{\mathrm{TH}} = 10$ mm	956	$A\#5$	$+27$

Table 1: Fundamental frequency, corresponding note and their pitch deviation in cents inside the synthetic instrument for the cases in the figure 9.

Finally, the experimental results reveal a quadratic scaling of the first harmonic frequency with respect to the tone hole diameter, as shown in dimensionless form in Fig. 10. The experimental points lie on the second-order polynomial with a R^2 coefficient of 0.9991 demonstrating the robustness of the quadratic law. The first two coefficients of the polynomial (shown in Fig. 10) are expected to depend on the geometry of the flute (mouthpiece and bore), on the distance of the TH from the labium, and on the mouth pressure. Further experiments are required in order to validate this scaling law.

The choice of the tone hole sizes and its position in the experiments was not aiming to generate specific notes. Nevertheless, Table 1 shows the note range corresponding to the frequency of the first harmonic for a musical interpretation. In particular, the notes range from $D5$ (fifth octave of D) in the closed tone hole case to $A\#5$ in the case of a 10 mm open tone hole. The deviation, computed in *Cent* (with 444 Hz tuning) [21] for the played notes, is also listed in Table 1.

4. DISCUSSION AND FUTURE WORK

Time-resolved PIV measurements are able to detect the vibration of the air column, and therefore the natural frequencies in the resonator of wind instruments. In the case of the simplified recorder examined in this study, the obtained frequencies for the flow oscillations are in agreement with those measured by pressure transducers inside the resonator. We therefore expect that PIV measurements can be used to analyse the acoustic behaviour of wind instruments in terms of fundamental frequencies and local effects arising by the presence of the tone holes. In addition, high-pass filters can be applied to the PIV data in order to focus the analysis on the fluctuations in acoustic regimes.

The present experimental campaign has investigated the influence of the tone hole size on the air-flow and its frequency content in the bore of the recorder for a given mouth pressure (100 Pa). Further PIV measurements are needed to characterize in detail the local flow effects (i.e., boundary layer separation, and vortex shedding). To this aim, the position of the PIV field of view should be placed at the edge of the tone hole and at the open end of the bore. In addition, the acquisition frequency can be reduced to detect only the first one or two harmonics in order to increase the field of view. Finally, to complete the scaling law of the fundamental frequency vs the TH diameter (presented in Section 3.3), it would be necessary to change the inlet pressure condition and the TH position. For the latter analysis, pressure transducers alone may also be used.

Such experimental measurements may increase our understanding of the tone hole influence on the flow inside wind instruments. Subsequently, a better understanding of tone hole effects can help to inform physical models for sound synthesis and sound analysis applications.

5. CONCLUSION

The effect of the tone hole size in wind instruments is investigated using time-resolved PIV measurements. The results show local peaks of the velocity fluctuations in the proximity of the TH, which are promoted by the jet streaming between the inner airflow and the external environment. At the open end of the instrument, the amplitude of the velocity fluctuations reduces with the size of the TH due to the pressure energy lost through the tone hole. Furthermore, comparisons with measurements using pressure transducers show that the harmonics of the flow can be obtained using PIV measurements. The fundamental frequencies detected inside the resonator of the recorder increase with the tone hole size. In particular, a quadratic scaling is found between the first harmonic of the natural frequencies and the diameter of the TH.

6. ACKNOWLEDGMENTS

This project has received funding from the European Union's Horizon 2020 research and innovation programme under the Marie Skłodowska-Curie grant agreement No 812719.

7. REFERENCES

[1] B. Fabre, J. Gilbert, A. Hirschberg, and X. Pelorson, "Aeroacoustics of musical instruments," *Annual review of fluid mechanics*, vol. 44, pp. 1–25, 2012.

[2] A. H. Benade, *Fundamentals of musical acoustics*. Courier Corporation, 1990.

[3] C. J. Nederveen, "Acoustical aspects of woodwind instruments," 1998.

[4] N. H. Fletcher and T. D. Rossing, *The Physics of Musical Instruments*. New York, NY: Springer New York, 1991.

[5] D. H. Keefe, "Experiments on the Single Woodwind Tone Hole," *The Journal of the Acoustical Society of America*, vol. 72, pp. 688–699, Sept. 1982.

[6] J.-P. Dalmont, C. J. Nederveen, and N. Joly, "Radiation impedance of tubes with different flanges: numerical and experimental investigations," *Journal of sound and vibration*, vol. 244, no. 3, pp. 505–534, 2001.

[7] R. Caussé, J. Kergomard, and X. Lurton, "Input impedance of brass musical instruments—comparison between experiment and numerical models," *The Journal of the Acoustical Society of America*, vol. 75, no. 1, pp. 241–254, 1984.

[8] D. H. Keefe, "Woodwind air column models," *The Journal of the Acoustical Society of America*, vol. 88, no. 1, pp. 35–51, 1990.

[9] D. H. Keefe, "Theory of the single woodwind tone hole," *The Journal of the Acoustical Society of America*, vol. 72, no. 3, pp. 676–687, 1982.

[10] V. Dubos, J. Kergomard, A. Khettabi, J.-P. Dalmont, D. Keefe, and C. Nederveen, "Theory of sound propagation in a duct with a branched tube using modal decomposition," *Acta Acustica united with Acustica*, vol. 85, no. 2, pp. 153–169, 1999.

[11] A. Lefebvre and G. P. Scavone, "Characterization of woodwind instrument toneholes with the finite element method," *The Journal of the Acoustical Society of America*, vol. 131, no. 4, pp. 3153–3163, 2012.

[12] V. Lorenzoni and D. Ragni, "Experimental investigation of the flow inside a saxophone mouthpiece by particle image velocimetry," *The Journal of the Acoustical Society of America*, vol. 131, no. 1, pp. 715–721, 2012.

[13] H. Yokoyama, A. Miki, H. Onitsuka, and A. Iida, "Direct numerical simulation of fluid–acoustic interactions in a recorder with tone holes," *The Journal of the Acoustical Society of America*, vol. 138, no. 2, pp. 858–873, 2015.

[14] D. J. Skulina, R. MacDonald, and D. M. Campbell, "PIV Applied to the Measurement of the Acoustic Particle Velocity at the Side Hole of a Duct," in *Forum Acusticum Conference*, p. 6, 2005.

[15] R. MacDonald, "Study of the undercutting of woodwind toneholes using particle image velocimetry," 2009.

[16] N. Giordano, "Nonlinear effects at woodwind toneholes," in *Proceedings of the International Symposium on Musical Acoustics*, 2014.

[17] G. C. Y. Lam, R. C. K. Leung, and S. K. Tang, "Aeroacoustics of T-junction merging flow," *J. Acoust. Soc. Am.*, vol. 133, no. 2, 2013.

[18] J. C. Bruggeman, A. Hirschberg, A. P. J. Wijnands, and J. Gorter, "Self-Sustained Aero-Acoustic Pulsations in Gas Transport Systems: Experimental Study of the Influence of Closed Side Branches," *Journal of Sound and Vibration*, 1991.

[19] C. F. Goss, "Intraoral pressure in ethnic wind instruments," *arXiv preprint arXiv:1308.5214*, 2013.

[20] J. Westerweel and F. Scarano, "Universal outlier detection for piv data," *Experiments in fluids*, vol. 39, pp. 1096–1100, 2005.

[21] B. H. Suits, *Physics Behind Music: An Introduction*. Cambridge University Press, 2023.